Path Following for Marine Surface Vessels

Morten Breivik and Thor I. Fossen
Centre for Ships and Ocean Structures (CESOS)
Norwegian University of Science and Technology (NTNU)
NO-7491 Trondheim, Norway
E-mail: morten.breivik@ieee.org, fossen@ieee.org

***Abstract*— This paper addresses the problem of path following for marine surface vessels by utilizing a novel guidance-based approach. The approach is equally applicable for land, sea and air vehicles. The main idea is to explicitly control the velocity vector of the vehicles in such a way that they converge to and follow desired geometrical paths in a natural and elegant manner. In this regard, all regular paths are feasible. A nonlinear model-based controller is designed for a fully actuated vessel to enable it to comply with the guidance commands. The vessel is exposed to a constant environmental force, hence integral action is added by means of parameter adaptation. By introducing sideslip compensation and a dynamic controller state, the results are extended to underactuated vessels.**

I. Introduction

When considering the task of traversing a given geometrical path, traditional trajectory tracking schemes mix the positional and temporal requirements into one single assignment even in the cases where the geometrical path is specified by a path planner and, as such, is completely known in advance. In this context, two weaknesses are apparent. Firstly, most of these schemes do not take advantage of geometrical information in the sense that they lapse into plain servosystem tracking of the position. This fact degrades the transient convergence behaviour of the position significantly, and makes it unnatural. Secondly, if the original time-parametrization of the path for some reason becomes dynamically infeasible, it must be awkwardly reparametrized to avoid an unstable system as a result of growing positional errors. In contrast to all of this, a human operating a vehicle does not aim at tracking a conceptual point in front of the vehicle, especially not if he understands that it is equivalent with risking lives or damaging the vehicle.

As an alternative to using traditional trajectory tracking for solving such problems, this paper presents a guidance-based path following scheme which takes advantage of geometrical information of the path whenever available. The approach also separates the positional and temporal requirements into two independent assignments. Specifically, the proposed approach is illustrated through the task of maneuvering marine surface vessels along a given path at sea.

This work was supported by the Research Council of Norway through the Centre for Ships and Ocean Structures at NTNU.

A. Previous Work

A lot of research has been carried out in the field of path following, especially in the field of wheeled mobile robots (WMR). A treatment of one of the most frequently used path following schemes can be found in a paper by Claude Samson [1]. The author considers a strategy of projecting the position of the actual WMR onto the desired geometrical path, effectively ensuring that an imagined, virtual vehicle exists on the position of the path which is closest to the real WMR at all times. This is achieved by applying the so-called Serret-Frenet equations, yielding the kinematics associated with the Serret-Frenet (SF) frame, which is the path tangential frame at the exact point of projection. The path following problem is then solved in the error space of this frame. However, there is a catch to this approach. Consider a path parametrized by its arc length s along the path. For every point along such a path, there exists an associated tangent circle with radius $r(s) = 1/c(s)$ where $c(s)$ is the curvature of the path. This circle is known as the osculating circle [2]. If at any time the WMR is located at the origin of the osculating circle, the projected point on the path will move infinitely fast. Hence, the SF kinematics contain a singularity at such a point. Samson solves this by restricting the position of the WMR to be contained inside a tube surrounding the path, with radius less than a minimum radius derived from the maximum path curvature. Such a restriction is obstructing, especially from a theoretical point-of-view, and effectively excludes the derivation of any global path following results. In addition to this, Samson has to apply Barbalat's lemma to prove convergence to the path. Consequently, only an asymptotic stability result can be claimed for the error variables.

In [3], a substantial improvement to the path following scheme from [1] is made. Instead of considering a SF frame attached to the exact point on the path which is closest to the WMR at all times, the origin of the SF frame is made to dynamically evolve according to a suitably defined function of time, thus removing the singularity previously associated with the SF kinematic equations. Consequently, a global result can be claimed. However, in the stability analysis of the proposed scheme the authors still have to resort to Barbalat's lemma, hence only asymptotic stability can be proven. In addition, the approach is restricted to arc-length parametrized paths, which are generally not trivial to deduce.

B. Main Contribution

This paper extends the results from [4] and presents a guidance-based path following scheme which is singularity-free for all regular paths. Hence, the considered geometrical paths are no longer only straight lines and circles. Furthermore, they are not required to be arc-length parametrized as in [1] and [3], and the path errors are proven to be either uniformly globally asymptotically and locally exponentially stable (UGAS/ULES) or uniformly globally exponentially stable (UGES), depending on the inherent limitations of the system to be controlled. The paper contains a lucid exposition of the proposed approach, which has an intuitive physical interpretation. Furthermore, UGAS/ULES is also proven for a closed loop system represented by a guided and controlled nonlinear dynamical model of a marine surface vessel. As in [4], the guidance and control framework in which the approach is developed easily extends from fully actuated to underactuated vessels, making path following feasible for the latter category as well.

II. Problem Statement

The primary objective in path following is to restrict the position of a vehicle to a specific manifold represented by a desired geometrical path, without any temporal requirements. The secondary objective is to ensure that the vehicle complies with a desired dynamical behaviour while traversing the path. By using the task classification scheme of [5], the path following problem can thus be expressed by the following two task objectives:

Geometric Task: Make the position of the vehicle converge to and follow a desired geometrical path.

Dynamic Task: Make the speed of the vehicle converge to and track a desired speed assignment.

The ability to accurately maneuver a vehicle along a given path is of primary importance for most applications, and the path following concept ensures such a prioritization.

III. Guidance System Design

The guidance system is a high-level decision-making system which gives commands to the control system. These commands are enforced through a set of actuators such that a given physical system behaves in a certain, desirable way. In this section, a guidance-based approach to solving the path following problem is presented. The theory is developed at the kinematic level to make it as general as possible, and is taken from [6] where it is treated more thoroughly.

A. Guidance Principle for a General Path

Consider a point mass particle situated on a two-dimensional surface. Denote the inertial position and velocity of this particle by $\mathbf{p} \in \mathbb{R}^2$ and $\mathbf{v} \in \mathbb{R}^2$, respectively. As all vectors, the velocity vector has two characteristics: size and orientation. Denote the size by $U = \|\mathbf{v}\|_2 = (\mathbf{v}^\intercal \mathbf{v})^{\frac{1}{2}}$ (the speed) and the orientation by $\chi = \arctan(\frac{v_y}{v_x})$ (the course). It is assumed that both U and χ can attain any desirable value instantaneously, consequently the point mass particle will be referred to as an ideal particle in what follows. Also defined on the two-dimensional surface is a geometrical path, parametrized by a scalar variable $\theta \in \mathbb{R}$. For any given θ, the inertial position of the geometrical path is denoted by $\mathbf{p}_d(\theta) \in \mathbb{R}^2$. The main objective is to make the ideal particle converge to and stay on this path, which can be achieved purely by controlling U and χ.

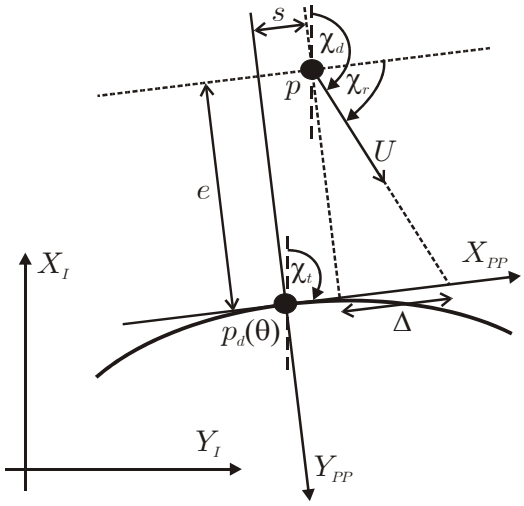

Fig. 1. The geometrical relationship between all the relevant parameters and variables utilized in the proposed guidance-based path following scheme.

For a given θ, define a local reference frame at $\mathbf{p}_d(\theta)$ and name it the Path Parallel (PP) frame. The PP frame is rotated an angle:

$$\chi_t(\theta) = \arctan\left(\frac{y_d'(\theta)}{x_d'(\theta)}\right) \tag{1}$$

relative to the inertial frame, where the notation $x_d'(\theta) = \frac{dx_d}{d\theta}(\theta)$ has been utilized. Consequently, the x-axis of the PP frame is aligned with the tangential vector to the path at $\mathbf{p}_d(\theta)$. The error vector between $\mathbf{p}$ and $\mathbf{p}_d(\theta)$ expressed in the PP frame is given by:

$$\boldsymbol{\varepsilon} = \mathbf{R}_p^\top(\chi_t)(\mathbf{p} - \mathbf{p}_d(\theta)), \tag{2}$$

where:

$$\mathbf{R}_p(\chi_t) = \begin{bmatrix} \cos\chi_t & -\sin\chi_t \\ \sin\chi_t & \cos\chi_t \end{bmatrix} \tag{3}$$

is the rotation matrix from the inertial frame to the PP frame, $\mathbf{R}_p \in SO(2)$. The error vector $\boldsymbol{\varepsilon} = [s, e]^\top$ consists of the along-track error s and the cross-track error e, see Figure 1. The along-track error represents the longitudinal distance to $\mathbf{p}_d(\theta)$ along the path-tangent at $\mathbf{p}_d(\theta)$, while the cross-track error represents the lateral distance to the path-tangent at $\mathbf{p}_d(\theta)$. A most convenient error space in which to operate is thus given by $\boldsymbol{\varepsilon} \in \mathbb{R}^2$, and since $\|\mathbf{R}_p\| = 1$ it is apparent that $\|\boldsymbol{\varepsilon}\| \to 0 \Leftrightarrow \|\mathbf{p} - \mathbf{p}_d(\theta)\| \to 0$. Consequently, the goal is to ensure that $\|\boldsymbol{\varepsilon}\| \to 0$ as $t \to \infty$ since this is identical to fulfilling the path following geometric task.

By differentiating $\boldsymbol{\varepsilon}$ with respect to time, we obtain:

$$\dot{\boldsymbol{\varepsilon}} = \dot{\mathbf{R}}_p^\top(\chi_t)(\mathbf{p} - \mathbf{p}_d) + \mathbf{R}_p^\top(\chi_t)(\dot{\mathbf{p}} - \dot{\mathbf{p}}_d), \tag{4}$$

where:

$$\dot{\mathbf{R}}_p(\chi_t) = \mathbf{R}_p(\chi_t)\mathbf{S}_p(\dot{\chi}_t) \tag{5}$$

with:

$$\mathbf{S}_p(\dot{\chi}_t) = \begin{bmatrix} 0 & -\dot{\chi}_t \\ \dot{\chi}_t & 0 \end{bmatrix}, \tag{6}$$

which is skew-symmetric; $\mathbf{S}_p(\dot{\chi}_t) = -\mathbf{S}_p^\top(\dot{\chi}_t)$. We also have that:

$$\dot{\mathbf{p}} = \mathbf{R}_p(\chi) \begin{bmatrix} U \\ 0 \end{bmatrix}, \tag{7}$$

where $\mathbf{R}_p(\chi)$ is the rotation matrix from the inertial frame to a body-fixed frame attached to the ideal particle with its x-axis along the velocity vector of the particle. Hence, the vector $[U, 0]^\top$ represents the ideal particle velocity with respect to the inertial frame, represented in such a body-fixed frame. In addition to this, we have that:

$$\dot{\mathbf{p}}_d = \mathbf{R}_p(\chi_t) \begin{bmatrix} U_{PP} \\ 0 \end{bmatrix}, \tag{8}$$

where $[U_{PP}, 0]^\top$ is the velocity of the PP frame with respect to the inertial frame, represented in the PP frame. Expanding (4), we get:

$$\begin{aligned} \dot{\boldsymbol{\varepsilon}} &= (\mathbf{R}_p(\chi_t)\mathbf{S}_p(\dot{\chi}_t))^\top(\mathbf{p} - \mathbf{p}_d) + \\ &\quad \mathbf{R}_p^\top(\chi_t)\left(\mathbf{R}_p(\chi)\begin{bmatrix} U \\ 0 \end{bmatrix} - \mathbf{R}_p(\chi_t)\begin{bmatrix} U_{PP} \\ 0 \end{bmatrix}\right), \end{aligned} \tag{9}$$

which can be simplified into:

$$\dot{\boldsymbol{\varepsilon}} = \mathbf{S}_p^\top(\dot{\chi}_t)\boldsymbol{\varepsilon} + \mathbf{R}_p(\chi - \chi_t)\begin{bmatrix} U \\ 0 \end{bmatrix} - \begin{bmatrix} U_{PP} \\ 0 \end{bmatrix} \tag{10}$$

since $\mathbf{R}_p^\top(\chi_t)\mathbf{R}_p(\chi) = \mathbf{R}_p(\chi - \chi_t)$.

Define the positive definite and radially unbounded Lyapunov function candidate (LFC):

$$V_\varepsilon = \frac{1}{2}\boldsymbol{\varepsilon}^\top\boldsymbol{\varepsilon} = \frac{1}{2}(s^2 + e^2) > 0, \tag{11}$$

and differentiate it with respect to time along the trajectories of $\boldsymbol{\varepsilon}$ to obtain:

$$\begin{aligned} \dot{V}_\varepsilon &= \boldsymbol{\varepsilon}^\top\dot{\boldsymbol{\varepsilon}} \\ &= \boldsymbol{\varepsilon}^\top\left(\mathbf{S}_p^\top(\dot{\chi}_t)\boldsymbol{\varepsilon} + \mathbf{R}_p(\chi - \chi_t)\begin{bmatrix} U \\ 0 \end{bmatrix}\right) - \\ &\quad \boldsymbol{\varepsilon}^\top\begin{bmatrix} U_{PP} \\ 0 \end{bmatrix} \\ &= \boldsymbol{\varepsilon}^\top\left(\mathbf{R}_p(\chi - \chi_t)\begin{bmatrix} U \\ 0 \end{bmatrix} - \begin{bmatrix} U_{PP} \\ 0 \end{bmatrix}\right) \end{aligned} \tag{12}$$

since the skew-symmetry of $\mathbf{S}_p(\dot{\chi}_t)$ leads to $\boldsymbol{\varepsilon}^\top\mathbf{S}_p^\top(\dot{\chi}_t)\boldsymbol{\varepsilon} = 0$. By further expansion, we get:

$$\dot{V}_\varepsilon = s(U\cos(\chi - \chi_t) - U_{PP}) + eU\sin(\chi - \chi_t). \tag{13}$$

We can consider the path tangential speed U_{PP} as a virtual input for stabilizing s. Consequently, by choosing U_{PP} as:

$$U_{PP} = U\cos(\chi - \chi_t) + \gamma s, \tag{14}$$

where $\gamma > 0$ becomes a gain parameter in the guidance law, we achieve:

$$\dot{V}_\varepsilon = -\gamma s^2 + eU\sin(\chi - \chi_t). \tag{15}$$

Since θ is the actual path parametrization variable that we can control for guidance purposes, we need to obtain a relationship between θ and U_{PP} to be able to implement (14). By using the kinematic relationship given by (8), we get that:

$$\begin{aligned} \dot{\theta} &= \frac{U_{PP}}{\sqrt{x_d'^2 + y_d'^2}} \\ &= \frac{U\cos(\chi - \chi_t) + \gamma s}{\sqrt{x_d'^2 + y_d'^2}}, \end{aligned} \tag{16}$$

which is nonsingular for all regular paths.

The next challenge is to stabilize the cross-track error e. Since we are dealing with an ideal particle, we can imagine that the course angle of its velocity vector is equal to a given desired course angle, i.e. $\chi = \chi_d$. Hence, the LFC derivative can be written as:

$$\dot{V}_\varepsilon = -\gamma s^2 + eU\sin(\chi_d - \chi_t), \tag{17}$$

where $(\chi_d - \chi_t)$ can be considered a virtual input for stabilizing e. Denote this angular difference by $\chi_r = \chi_d - \chi_t$, i.e. the relative angle between the desired course and the path tangential course. Obviously, such a variable should depend on e, such that $\chi_r = \chi_r(e)$. An attractive choice for $\chi_r(e)$ would be the physically motivated:

$$\chi_r(e) = \arctan\left(-\frac{e}{\triangle}\right), \tag{18}$$

where $\triangle > 0$ becomes a guidance parameter utilized to shape the convergence towards the path tangential. It is often referred to as the lookahead distance in literature dealing with path following along straight lines [7], and the physical interpretation can be derived from Figure 1. Note that other $\arctan$-like shaping functions are also possible candidates for $\chi_r(e)$, for instance the $\tanh$ function.

By choosing $\chi_r(e)$ as in (18), the derivative of the LFC finally becomes:

$$\begin{aligned} \dot{V}_\varepsilon &= -\gamma s^2 + eU\sin(\chi_r) \\ &= -\gamma s^2 - \frac{Ue^2}{\sqrt{e^2 + \triangle^2}}, \end{aligned} \tag{19}$$

which is negative definite for non-zero speeds $U > 0$, hence the LFC is a Lyapunov function. The last transition is easily made by utilizing trigonometrical relationships from Figure 1. Note that the speed by definition cannot be negative.

To sum up, the desired course angle which χ should equal is given by:

$$\chi_d(\theta, e) = \chi_t(\theta) + \chi_r(e) \tag{20}$$

with $\chi_t(\theta)$ as in (1) and $\chi_r(e)$ as in (18).

The result represented by (19) is intuitively obvious since the along-track error will converge to zero regardless of whether the ideal particle is moving or not, due to the assigned dynamics in (16). The cross-track error, however, relies on a non-zero particle speed.

The following proposition can now be stated:

Proposition 1: The origin $\boldsymbol{\varepsilon} = \mathbf{0}$ is uniformly globally asymptotically and locally exponentially stable (UGAS/ULES) if θ is updated by (16), χ is equal to (20) and U is required to be non-zero and bounded from below.

Proof: The Lyapunov function given by (11) is positive definite and radially unbounded, while its derivative with respect to time (19) is negative definite when adhering to (16), (20) and $U \geq U_{\min} > 0$. Hence, by standard Lyapunov arguments the origin $\boldsymbol{\varepsilon} = \mathbf{0}$ is UGAS. Furthermore, the Jacobian of the error dynamics at the origin has strictly negative eigenvalues, which proves ULES. Note that the region of ULES depends on $\triangle$. ■

By stabilizing $\boldsymbol{\varepsilon} = \mathbf{0}$, we have achieved the path following geometric task. The dynamic task is satisfied by making sure that $U = U_d$, where $U_d \geq U_{d,\min} > 0$.

Note that by choosing the speed of the particle equal to:

$$U = \kappa \sqrt{e^2 + \triangle^2}, \tag{21}$$

where $\kappa > 0$, we obtain:

$$\dot{V}_{\varepsilon} = -\gamma s^2 - \kappa e^2 < 0, \tag{22}$$

which results in the following proposition:

Proposition 2: The origin $\boldsymbol{\varepsilon} = \mathbf{0}$ is uniformly globally exponentially stable (UGES) if θ is updated by (16), χ is equal to (20) and U satisfies (21).

Proof: The Lyapunov function given by (11) is positive definite and radially unbounded, while its derivative with respect to time (22) is quadratically negative definite when adhering to (16), (20) and (21). Hence, by standard Lyapunov arguments the origin $\boldsymbol{\varepsilon} = \mathbf{0}$ is UGES. ■

This is indeed a very strong result, but clearly not achievable by physical systems since these exhibit natural limitations on their maximum attainable speed. In this regard, proposition 1 states the best possible stability property a physical system, like a marine surface vessel, can hold.

B. The Role of the Guidance System

A simplified illustration of the main components required for controlling a marine surface vessel is given in Figure 2. The navigation system is composed of an array of sensors feeding their raw data to an observer; an advanced signal processing algorithm with dead-reckoning capability. The guidance system computes all the reference signals necessary to make the physical system autonomous, and feeds these to the control system. In turn, the control system carries out the instructions given by the guidance system. It consists of the control law and the control allocation scheme, which distributes the commanded forces and moments to the vessel actuators. It is important to recognize the fact that if the underlying guidance principles

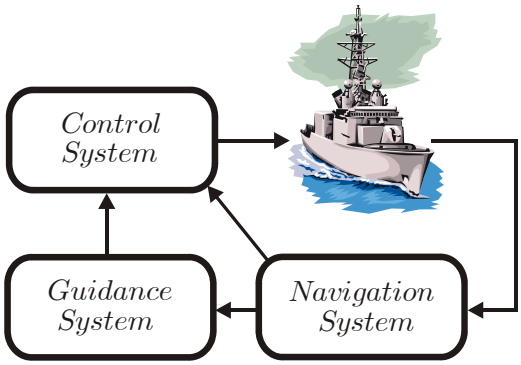

Fig. 2. The key components necessary for controlling a marine surface vessel.

upon which the guidance system is based are insufficient in some sense, the best control system in the world cannot save the physical system from performing poorly. Therefore, extra care should be put into designing the guidance system. Note that the guidance principle treated in this paper only represents what lies at the core of a guidance system, which in itself consists of a plethora of algorithms designed to make a physical system as autonomous as possible.

C. Considerations towards Underactuation

An underactuated vessel, also termed a second order nonholonomic system, has fewer directionally independent control inputs available simultaneously than there are number of degrees-of-freedom (DOF) to be controlled. This paper considers the maneuvering of marine surface vessels by a path following approach, which by its very nature holds several advantageous properties from a nonholonomic perspective. When combined with a guidance principle which redefines the output-to-be-controlled from 3 DOF position and heading to 2 DOF speed and heading [8], a very favourable design approach for a certain type of underactuated vessels emerge. While being underactuated in the original 3 DOF configuration space, these vessels are no longer underactuated in the redefined 2 DOF one. Hence, the problem has been recast into one which is no longer underactuated in terms of the variables to be controlled, and which nevertheless through the guidance principle ensures the primary goal of positional convergence. The approach becomes equally attractive for both fully actuated and underactuated vessels when in addition elegant and energy efficient convergence behaviour is guaranteed.

As defined in [4], the course angle χ is the orientation of the velocity vector of a vessel, the heading angle ψ is the orientation of the vessel itself, while the sideslip angle β is the difference between the course angle and the heading angle. The heading angle equals the course angle ($\psi = \chi$) when the sway speed is zero ($v = 0$), i.e. when there is no sideslip. This is generally attainable for fully actuated vessels, but not for those which are unactuated in the sway direction. Specifically, to achieve path following for such vessels, the heading angle must be actively used to direct the velocity vector in the desired direction by using so-called sideslip compensation.

Hence, the vessel acts as a weather vane with an uncontrollable vessel speed $U = \sqrt{u^2 + v^2}$, a quality which is not possible to alleviate. Such a feature represents an inherent limitation of sway-underactuated vessels, for which the dynamic task cannot be perfectly satisfied. In practice however, the surge speed is much greater than the sway speed; $U \approx u$. The primary objective is nevertheless the geometric task, which is perfectly achievable.

Sideslip compensation essentially means that the desired heading angle must be computed by:

$$\psi_d = \chi_d - \beta, \tag{23}$$

where higher order derivatives are generated by processing ψ_d through a reference model which is adjusted to the closed loop vessel dynamics.

IV. Control System Design

It is usually sufficient to consider only the 3 horizontal DOFs when designing control systems for surface vessels since for most of them, the low frequency vertical plane dynamics and the thruster action does not influence each other [9].

A. Model of a Marine Surface Vessel

The 3 DOF kinematics and kinetics of a marine surface vessel can be represented as [10]:

$$\dot{\boldsymbol{\eta}} = \mathbf{R}(\psi)\boldsymbol{\nu} \tag{24}$$

and:

$$\mathbf{M}\dot{\boldsymbol{\nu}} + \mathbf{C}(\boldsymbol{\nu})\boldsymbol{\nu} + \mathbf{D}(\boldsymbol{\nu})\boldsymbol{\nu} = \boldsymbol{\tau} + \mathbf{R}(\psi)^\top \mathbf{b}, \tag{25}$$

where $\boldsymbol{\eta} = [x, y, \psi]^\top \in \mathbb{R}^2 \times [-\pi, \pi]$ represents the earth-fixed position and heading, $\boldsymbol{\nu} = [u, v, r]^\top \in \mathbb{R}^3$ represents the vessel-fixed velocities, $\mathbf{R}(\psi) \in SO(3)$ is the rotation matrix from the earth-fixed local geographic reference frame (NED) to the vessel-fixed reference frame (BODY), $\mathbf{M}$ is the vessel inertia matrix, $\mathbf{C}(\boldsymbol{\nu})$ is the centrifugal and coriolis matrix, $\mathbf{D}(\boldsymbol{\nu})$ is the hydrodynamic damping matrix, $\boldsymbol{\tau}$ represents the vessel-fixed propulsion forces and moments, and $\mathbf{b}$ describes the earth-fixed low frequency (LF) environmental forces acting on the vessel. These are caused by wind, current and second order wave loads, and are so low frequent compared to the vessel dynamics that $\dot{\mathbf{b}} = \mathbf{0}$ is a valid assumption. Such forces can be counteracted by the propulsion devices of the vessel, while high frequency (HF) first order wave-induced forces cannot. Hence, any motion components caused by HF forces must be removed from the vessel measurements before they can enter the control loop. This avoids unnecessary wear and tear of the propulsion system [10]. The necessary filtering of HF components are assumed to be taken care of.

The system matrices in (25) are assumed to satisfy the properties $\mathbf{M} = \mathbf{M}^\top > 0$, $\mathbf{C} = -\mathbf{C}^\top$ and $\mathbf{D} > 0$. Note that the symmetry property of $\mathbf{M}$ is destroyed at higher speeds due to the effect of hydrodynamically added mass. Still, a symmetric inertia matrix can be obtained by the utilization of acceleration feedback as described in [11]. Consequently, the assumption is considered to be valid. Also, the skew-symmetric property of the $\mathbf{C}$ matrix simply implies the physical fact that centrifugal and coriolis forces and moments contribute nothing to the kinetic energy of the vessel. Finally, note the positiveness property of the damping matrix $\mathbf{D}$. This is a property which should be utilized when designing controllers by carefully avoiding cancellation of valuable damping terms by the control law.

Specifically, the system matrices are defined as in [12], except for the assumption that the vessel has port-starboard symmetry. However, this is highly valid for most cases, whereas an additional assumption of fore-aft symmetry, as in [13], is far more questionable because it implies uncoupled sway and yaw dynamics.

B. Control Law Design

A control law is designed for a fully actuated marine surface vessel, and kept valid for a sway-underactuated vessel by introducing a dynamic controller state.

1) Fully Actuated Marine Surface Vessels: A fully actuated vessel is able to command independent accelerations in all relevant DOFs simultaneously. Consequently, the control vector of a fully actuated surface vessel is given by:

$$\boldsymbol{\tau} = [\tau_1, \tau_2, \tau_3]^\top, \tag{26}$$

where τ_1 represents the force input in surge, τ_2 represents the force input in sway, and τ_3 represents the moment input in yaw.

The model-based control law is deduced by using the backstepping technique for nonlinear dynamical systems [14]. The design is performed in two steps, and is an extension of the work already presented in [15]. Specifically, a more complex vessel model, together with environmental disturbances, are considered. Care is now taken to avoid cancellation of valuable hydrodynamical damping terms by the control law. It is assumed that a control allocation algorithm is readily available to efficiently distribute the controller force and moment commands to the specific actuators of the vessel [16].

The reference signals needed for control are the desired heading angle and its higher order derivatives ψ_d, $\dot{\psi}_d$ and $\ddot{\psi}_d$, and the desired surge speed and its derivative u_d, $\dot{u}_d$. The heading signals are delivered by a guidance system as presented in section III, while the speed signals are given by a human operator, for instance through a path speed profile planner. All reference signals are assumed to be bounded, i.e. they belong to the signal space $\mathcal{L}_\infty$.

Start by defining the projection vector $\mathbf{h}$:

$$\mathbf{h} \triangleq [0, 0, 1]^\top, \tag{27}$$

then the error variables $z_1 \in \mathbb{R}$ and $\mathbf{z}_2 \in \mathbb{R}^3$ according to:

$$z_1 \triangleq \psi - \psi_d = \mathbf{h}^\top \boldsymbol{\eta} - \psi_d \tag{28}$$

$$\mathbf{z}_2 \triangleq [z_{2,1}, z_{2,2}, z_{2,3}]^\top = \boldsymbol{\nu} - \boldsymbol{\alpha}, \tag{29}$$

where $\boldsymbol{\alpha} = [\alpha_1, \alpha_2, \alpha_3]^\top \in \mathbb{R}^3$ is a vector of stabilizing functions to be specified later.

Step 1:

Define the first Control Lyapunov Function (CLF) as:

$$V_1 \triangleq \frac{1}{2} z_1^2 > 0. \tag{30}$$

Differentiating V_1 with respect to time along the z_1-dynamics yields:

$$\begin{aligned} \dot{V}_1 &= z_1 \dot{z}_1 \\ &= z_1(\mathbf{h}^\top \dot{\boldsymbol{\eta}} - \dot{\psi}_d) \\ &= z_1(\mathbf{h}^\top \boldsymbol{\nu} - \dot{\psi}_d) \end{aligned} \tag{31}$$

since $\dot{\boldsymbol{\eta}} = \mathbf{R}\boldsymbol{\nu}$ and $\mathbf{h}^T\mathbf{R}\boldsymbol{\nu} = \mathbf{h}^T\boldsymbol{\nu}$. By using (29), we obtain:

$$\begin{aligned} \dot{V}_1 &= z_1(\mathbf{h}^\top(\mathbf{z}_2 + \boldsymbol{\alpha}) - \dot{\psi}_d) \\ &= z_1\mathbf{h}^\top\mathbf{z}_2 + z_1(\mathbf{h}^\top\boldsymbol{\alpha} - \dot{\psi}_d) \\ &= z_1\mathbf{h}^\top\mathbf{z}_2 + z_1(\alpha_3 - \dot{\psi}_d). \end{aligned} \tag{32}$$

This motivates the choice of the stabilizing function α_3 as:

$$\alpha_3 = -k_1 z_1 + \dot{\psi}_d, \tag{33}$$

where $k_1 > 0$, which results in:

$$\dot{V}_1 = -k_1 z_1^2 + z_1\mathbf{h}^\top\mathbf{z}_2. \tag{34}$$

This concludes Step 1.

Step 2:

Augment the first CLF to obtain:

$$V_2 \triangleq V_1 + \frac{1}{2}\mathbf{z}_2^\top\mathbf{M}\mathbf{z}_2 + \frac{1}{2}\tilde{\mathbf{b}}^\top\boldsymbol{\Gamma}^{-1}\tilde{\mathbf{b}} > 0, \tag{35}$$

where $\tilde{\mathbf{b}} \in \mathbb{R}^3$ is an adaptation error defined as $\tilde{\mathbf{b}} = \hat{\mathbf{b}} - \mathbf{b}$ with $\hat{\mathbf{b}}$ being the estimate of the environmental disturbance vector $\mathbf{b}$, and by assumption $\dot{\mathbf{b}} = \mathbf{0}$. $\boldsymbol{\Gamma} = \boldsymbol{\Gamma}^\top > 0$ is the adaptation gain matrix.

Differentiating V_2 along the trajectories of z_1, $\mathbf{z}_2$ and $\tilde{\mathbf{b}}$, we obtain:

$$\dot{V}_2 = -k_1 z_1^2 + z_1\mathbf{h}^\top\mathbf{z}_2 + \mathbf{z}_2^\top\mathbf{M}\dot{\mathbf{z}}_2 + \tilde{\mathbf{b}}^\top\boldsymbol{\Gamma}^{-1}\dot{\tilde{\mathbf{b}}} \tag{36}$$

since $\mathbf{M} = \mathbf{M}^\top$ and $\dot{\tilde{\mathbf{b}}} = \dot{\hat{\mathbf{b}}}$. The fact that:

$$\begin{aligned} \mathbf{M}\dot{\mathbf{z}}_2 &= \mathbf{M}(\dot{\boldsymbol{\nu}} - \dot{\boldsymbol{\alpha}}) \\ &= \boldsymbol{\tau} + \mathbf{R}^\top\mathbf{b} - \mathbf{C}(\boldsymbol{\nu})\boldsymbol{\nu} - \mathbf{D}(\boldsymbol{\nu})\boldsymbol{\nu} - \mathbf{M}\dot{\boldsymbol{\alpha}} \end{aligned} \tag{37}$$

yields:

$$\begin{aligned} \dot{V}_2 = &-k_1 z_1^2 + \mathbf{z}_2^\top(\mathbf{h}z_1 + \boldsymbol{\tau} + \mathbf{R}^\top\mathbf{b} - \mathbf{C}(\boldsymbol{\nu})\boldsymbol{\nu}) + \\ &\mathbf{z}_2^\top(-\mathbf{D}(\boldsymbol{\nu})\boldsymbol{\nu} - \mathbf{M}\dot{\boldsymbol{\alpha}}) + \tilde{\mathbf{b}}^\top\boldsymbol{\Gamma}^{-1}\dot{\tilde{\mathbf{b}}}. \end{aligned} \tag{38}$$

By rewriting $\mathbf{C}(\boldsymbol{\nu}) = \mathbf{C}$ and $\mathbf{D}(\boldsymbol{\nu}) = \mathbf{D}$ for notational brevity, and utilizing the fact that $\boldsymbol{\nu} = \mathbf{z}_2 + \boldsymbol{\alpha}$ and $\mathbf{b} = \hat{\mathbf{b}} - \tilde{\mathbf{b}}$, we obtain:

$$\begin{aligned} \dot{V}_2 = &-k_1 z_1^2 - \mathbf{z}_2^\top\mathbf{C}\mathbf{z}_2 - \mathbf{z}_2^\top\mathbf{D}\mathbf{z}_2 + \\ &\mathbf{z}_2^\top(\mathbf{h}z_1 + \boldsymbol{\tau} + \mathbf{R}^\top\hat{\mathbf{b}} - \mathbf{C}\boldsymbol{\alpha} - \mathbf{D}\boldsymbol{\alpha} - \mathbf{M}\dot{\boldsymbol{\alpha}}) + \\ &\tilde{\mathbf{b}}^\top\boldsymbol{\Gamma}^{-1}(\dot{\hat{\mathbf{b}}} - \boldsymbol{\Gamma}\mathbf{R}\mathbf{z}_2), \end{aligned} \tag{39}$$

where $\mathbf{z}_2^\top\mathbf{C}\mathbf{z}_2 = 0$ because $\mathbf{C}$ is skew-symmetric [10]. By assigning:

$$\boldsymbol{\tau} = \mathbf{M}\dot{\boldsymbol{\alpha}} + \mathbf{C}\boldsymbol{\alpha} + \mathbf{D}\boldsymbol{\alpha} - \mathbf{R}^\top\hat{\mathbf{b}} - \mathbf{h}z_1 - \mathbf{K}_2\mathbf{z}_2, \tag{40}$$

where $\mathbf{K}_2 = diag(k_{2,1}, k_{2,2}, k_{2,3}) > 0$, and by choosing:

$$\dot{\hat{\mathbf{b}}} = \boldsymbol{\Gamma}\mathbf{R}\mathbf{z}_2, \tag{41}$$

we finally obtain:

$$\dot{V}_2 = -k_1 z_1^2 - \mathbf{z}_2^\top(\mathbf{D} + \mathbf{K}_2)\mathbf{z}_2 \leq 0, \tag{42}$$

where the inherent damping properties of the system have been preserved.

Currently, α_3 is the only stabilizing function which has been defined. Since we want the surge speed of the vessel to track a given speed assignment, we choose $\alpha_1 = u_d$. It is also desirable that the sway velocity of the vessel is kept identically at zero, such that the vessel traverses the path with its heading aligned with the path tangential vector. Consequently, we assign $\alpha_2 = 0$, which is feasible since the sway direction of the vessel is actuated. Hence, we obtain:

$$\boldsymbol{\alpha} = \left[u_d, 0, -k_1 z_1 + \dot{\psi}_d\right]^\top. \tag{43}$$

The main result of the control law design is summarized by the following proposition:

Proposition 3: For smooth reference trajectories ψ_d, $\dot{\psi}_d$ and $\ddot{\psi}_d \in \mathcal{L}_\infty$ and u_d, $\dot{u}_d \in \mathcal{L}_\infty$, the origin of the error system $(z_1, \mathbf{z}_2, \tilde{\mathbf{b}})$ becomes uniformly globally asymptotically and locally exponentially stable (UGAS/ULES) by choosing the control and disturbance adaptation laws as in (40) and (41), respectively.

Proof: See [17], utilizing Theorem A.5 from [10]. ■

Note that proposition 3 in itself tells us nothing about the path following capability of a vessel controlled by (40) and (41) since it only concerns the origin $(z_1, \mathbf{z}_2, \tilde{\mathbf{b}}) = \mathbf{0}$. Section V addresses such a capability.

2) Underactuated Marine Surface Vessels: We consider underactuation in the sway direction:

$$\boldsymbol{\tau} = [\tau_1, 0, \tau_3]^\top, \tag{44}$$

which represents the most common actuator configuration among vessels travelling at high speed.

Since τ_2 is not available to implement the required terms for the sway direction, dynamics can be imposed on the corresponding stabilizing function such that (40) is still satisfied [15]. By simultaneously utilizing sideslip compensation as described by (23), path following capability is maintained.

In our particular case, an analysis of the resulting α_2-subsystem reveals that the sway speed of the underactuated vessel remains bounded. Note that an analysis of what happens to v seldom is performed for underactuated vessels. Traditionally, this is the practice in literature treating autopilot design by using the Nomoto model [10], but even nonlinear control design concepts disregard the analysis, see e.g. [3].

Sway-underactuated vessels are extensively treated in the literature. Most approaches only consider diagonal system matrices and no environmental disturbances. However, [18] lifts these assumptions. Unfortunately, exact path following for an arbitrary point cannot be achieved by this approach since it requires the controlled point to be located where the system

matrices become diagonal. Also, u is required to exceed v. Such restrictions are not imposed in this paper. In fact, any point on the vessel can be controlled, and the scheme only requires the surge speed to be non-zero.

V. Closed Loop Behaviour of a Guided and Controlled Marine Surface Vessel

Consider the state vector $\mathbf{x}$ representing the total error system for a guided and controlled marine surface vessel:

$$\mathbf{x} = \left[\boldsymbol{\varepsilon}^\top, \mathbf{z}^\top, \tilde{\mathbf{b}}^\top\right]^\top \in \mathbb{R}^9, \tag{45}$$

where $\mathbf{z} \triangleq \left[z_1, \mathbf{z}_2^\top\right]^\top$. The following theorem can now be stated:

Theorem 1: The origin $\mathbf{x} = \mathbf{0}$ is uniformly globally asymptotically and locally exponentially stable (UGAS/ULES) if the path parametrization variable θ is updated by (16), the desired course angle χ_d is given by (20), the desired surge speed is selected as $|u_d| \geq |u_{d,\min}| > 0$, and the control and disturbance adaptation laws are given by (40) and (41), respectively.

Proof: The analysis is carried out by recognizing the closed loop dynamics of a guided and controlled marine surface vessel as a cascaded interconnection between the guidance and control subsystems, as depicted in Figure 3. In this regard, consider the Lyapunov-like function for the $(\mathbf{z}, \tilde{\mathbf{b}})$-subsystem (the control subsystem):

$$V_{\mathbf{z},\tilde{\mathbf{b}}} = \frac{1}{2}(z_1^2 + \mathbf{z}_2^\top \mathbf{M}\mathbf{z}_2 + \tilde{\mathbf{b}}^\top \boldsymbol{\Gamma}^{-1}\tilde{\mathbf{b}}) > 0 \tag{46}$$

and its derivative along the dynamics of this subsystem:

$$\dot{V}_{\mathbf{z},\tilde{\mathbf{b}}} = -k_1 z_1^2 - \mathbf{z}_2^\top(\mathbf{D} + \mathbf{K}_2)\mathbf{z}_2 \leq 0, \tag{47}$$

resulting from choosing the control and disturbance adaptation laws as (40) and (41), respectively. Proposition 3 states that the origin $(\mathbf{z}, \tilde{\mathbf{b}}) = \mathbf{0}$ of this subsystem is UGAS/ULES. This is so regardless of the $\boldsymbol{\varepsilon}$-subsystem.

Then consider the Lyapunov-like function for the $\boldsymbol{\varepsilon}$-subsystem (the guidance subsystem):

$$V_\varepsilon = \frac{1}{2}\boldsymbol{\varepsilon}^\top \boldsymbol{\varepsilon} > 0 \tag{48}$$

and its derivative along the dynamics of this subsystem:

$$\dot{V}_\varepsilon = -\gamma s^2 + eU\sin(\chi - \chi_t), \tag{49}$$

resulting from updating the path parametrization variable θ by (16). Now, rewrite χ as $\chi = \chi - \chi_d + \chi_d = z_1 + \chi_d$. By inserting this into (49), we obtain:

$$\dot{V}_\varepsilon = -\gamma s^2 + eU\sin(\chi_r + z_1) \tag{50}$$

since $\chi_d - \chi_t = \chi_r$, which is valid because the desired course angle χ_d is chosen as (20).

This expression can be expanded further by utilizing the trigonometric relationship:

$$\sin(\chi_r + z_1) = \sin(\chi_r)\cos(z_1) + \cos(\chi_r)\sin(z_1), \tag{51}$$

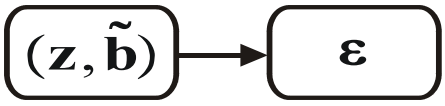

Fig. 3. A simplified overview illustrating the cascaded structure of a guided and controlled marine surface vessel.

which results in:

$$\begin{aligned}\dot{V}_\varepsilon &= -\gamma s^2 + eU(\sin(\chi_r)\cos(z_1) + \cos(\chi_r)\sin(z_1)) \\ &= -\gamma s^2 + \\ &\quad -\frac{Ue^2}{\sqrt{e^2+\triangle^2}}\cos(z_1) + \frac{U\triangle e}{\sqrt{e^2+\triangle^2}}\sin(z_1)\end{aligned} \tag{52}$$

by utilizing additional trigonometrical relationships from Figure 1. Finally:

$$\dot{V}_\varepsilon = -\gamma s^2 - \frac{U}{\sqrt{e^2+\triangle^2}}\left(e^2\cos(z_1) - \triangle e\sin(z_1)\right) \tag{53}$$

Clearly, there exists a finite time $t_1 \geq t_o \geq 0$ at which $U \geq U_{\min} > 0\ \forall t \geq t_1$ since $|u_d| \geq |u_{d,\min}| > 0$. Accordingly, there exists a finite time $t_2 \geq t_1$ at which $|z_1| \leq |z_{1,ss}|$ where $z_{1,ss} \Leftrightarrow \dot{V}_\varepsilon < 0$. During the time $t_1 - t_2$, $\dot{V}_\varepsilon \geq 0$ by definition. Since all the forcing terms U, $\cos(z_1)$ and $\sin(z_1)$ belong to $\mathcal{L}_\infty$, the solutions of ε are bounded over this time interval. Consequently, $\boldsymbol{\varepsilon} \to 0$ as $t \to \infty$ for any $\boldsymbol{\varepsilon}_0 \in \mathbb{R}^2$. The response is also uniform in t_0, hence the states of the forced $\boldsymbol{\varepsilon}$-subsystem are uniformly globally bounded (UGB). Therefore, $\mathbf{x}$ is UGB since the states belonging to the $(\mathbf{z}, \tilde{\mathbf{b}})$-subsystem are UGB. A standard result from cascade theory can now be applied to conclude UGAS of the cascade:

$$UGAS_{\mathbf{z},\tilde{\mathbf{b}}} + UGAS_{\boldsymbol{\varepsilon},unforced} + UGB_{\mathbf{x}} \Leftrightarrow UGAS_{\mathbf{x}}, \tag{54}$$

see e.g. [19]. Furthermore, the origin $\mathbf{x} = \mathbf{0}$ can be shown to be an exponentially stable equilibrium point of the linear, time-varying system resulting from linearizing the nonlinear $\mathbf{x}$-dynamics around $\mathbf{x} = \mathbf{0}$, giving ULES. ■

Theorem 1 shows that the closed loop system of the marine surface vessel fulfils the path following task objectives as stated in section II.

VI. Case Study: An Underactuated Marine Surface Vessel

A simulation is performed with an underactuated marine surface vessel, unactuated in the sway direction, trying to follow a sinusoidal path while being exposed to a constant environmental force. The vessel data comes from the model ship Cybership 2, a 1:70 scale model of a supply vessel, which has a mass of $m = 23.8\ kg$ and a length of $L = 1.255\ m$ [12]. The desired geometrical path is a sinusoid expressed as $\mathbf{p}_d(\theta) = \left[A\sin(\frac{\theta}{\lambda}), \theta\right]^\top$ with $A = 10$ and $\lambda = 15$. The environmental disturbance acts from the northwest with a size of about $1.4\ N$. Specifically, $\mathbf{b} = [-1\ (N), 1\ (N), 0\ (Nm)]^\top$.

The initial vessel states are chosen to be $\boldsymbol{\eta}_0 = [-10\ (m), 3\ (m), 0.785\ (rad)]^\top$ and $\boldsymbol{\nu}_0 = [0.25\ (m/s), 0\ (m/s), 0\ (rad/s)]^\top$, where the initial

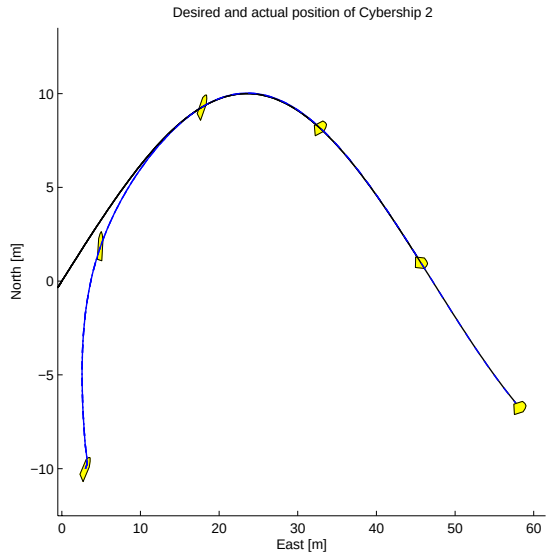

Fig. 4. Cybership 2 converges naturally to the desired geometrical path.

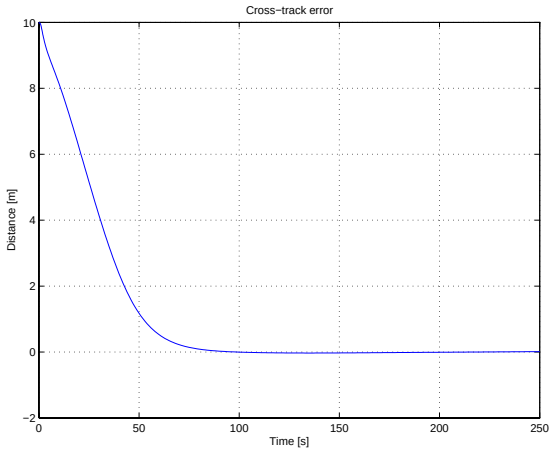

Fig. 5. The cross-track error converges to zero.

surge speed is to be kept during the run. The initial path parametrization variable is set to $\theta_0 = 0$ and the guidance parameter is $\gamma = 100$. The lookahead distance in the guidance law is chosen to be $\triangle = 3L$. The controller gains are chosen as $k_1 = 10$, $k_{2,1} = 10$, $k_{2,2} = 1$ and $k_{2,3} = 10$, while $\mathbf{\Gamma} = \mathbf{I}$.

Figure 4 shows that the vessel converges elegantly to the path, which would have been impossible without sideslip compensation since the vessel is unactuated in the sway direction. Figure 5 illustrates that the cross-track error converges to zero.

VII. Conclusion

This paper has presented a novel guidance-based path following approach to maneuvering marine surface vessels. The approach guarantees positional convergence to a desired geometrical path, and is equally applicable to land, sea and air vehicles. Furthermore, a nonlinear model-based controller has been designed for a fully actuated vessel such that it can comply with the guidance commands. Since the vessel is exposed to a constant environmental force, integral action is added to the controller by means of a parameter adaptation technique. By introducing sideslip compensation and a dynamic controller state, the results are extended to underactuated vessels which are unactuated in the sway direction. The total contribution is a guidance and control scheme which fulfils the path following objective for both fully actuated and underactuated marine surface vessels. Simulation results successfully demonstrate the capability of the proposed guidance and control strategy.

Acknowledgments

The authors would like to thank colleagues at the Centre for Ships and Ocean Structures and the Department of Engineering Cybernetics at NTNU for constructive comments and suggestions.

References

[1] C. Samson, "Path following and time-varying feedback stabilization of a wheeled mobile robot," in *Proceedings of the ICARCV'92, Singapore*, 1992.

[2] R. Skjetne and T. I. Fossen, "Nonlinear maneuvering and control of ships," in *Proceedings of the MTS/IEEE OCEANS, Honolulu, Hawaii, USA*, 2001.

[3] L. Lapierre, D. Soetanto, and A. Pascoal, "Nonlinear path following with applications to the control of autonomous underwater vehicles," in *Proceedings of the 42nd IEEE CDC, Maui, Hawaii, USA*, 2003.

[4] M. Breivik and T. I. Fossen, "Path following of straight lines and circles for marine surface vessels," in *Proceedings of the 6th IFAC CAMS, Ancona, Italy*, 2004.

[5] R. Skjetne, T. I. Fossen, and P. V. Kokotović, "Robust output maneuvering for a class of nonlinear systems," *Automatica*, vol. 40, no. 3, pp. 373–383, 2004.

[6] M. Breivik and T. I. Fossen, "Guidance for path following and trajectory tracking," in progress.

[7] F. A. Papoulias, "Bifurcation analysis of line of sight vehicle guidance using sliding modes," *International Journal of Bifurcation and Chaos*, vol. 1, no. 4, pp. 849–865, 1991.

[8] A. J. Healey and D. B. Marco, "Slow speed flight control of autonomous underwater vehicles: Experimental results with the NPS AUV II," in *Proceedings of the 2nd ISOPE, San Francisco, California, USA*, 1992.

[9] A. J. Sørensen, *Marine Cybernetics: Modelling and Control*, 2nd ed. Marine Technology Centre, Trondheim, Norway, 2002.

[10] T. I. Fossen, *Marine Control Systems: Guidance, Navigation and Control of Ships, Rigs and Underwater Vehicles*, 1st ed. Marine Cybernetics, Trondheim, Norway, 2002.

[11] T. I. Fossen, K. P. Lindegaard, and R. Skjetne, "Inertia shaping techniques for marine vessels using acceleration feedback," in *Proceedings of the 15th IFAC World Congress on Automatic Control, Barcelona, Spain*, 2002.

[12] R. Skjetne, Ø. N. Smogeli, and T. I. Fossen, "A nonlinear ship manoeuvering model: Identification and adaptive control with experiments for a model ship," *Modeling, Identification and Control*, vol. 25, no. 1, pp. 3–27, 2004.

[13] K. Y. Pettersen and E. Lefeber, "Way-point tracking control of ships," in *Proceedings of the 40th IEEE CDC, Orlando, Florida, USA*, 2001.

[14] M. Krstić, I. Kanellakopoulos, and P. V. Kokotović, *Nonlinear and Adaptive Control Design*. John Wiley & Sons Inc., 1995.

[15] T. I. Fossen, M. Breivik, and R. Skjetne, "Line-of-sight path following of underactuated marine craft," in *Proceedings of the 6th IFAC MCMC, Girona, Spain*, 2003.

[16] T. A. Johansen, "Optimizing nonlinear control allocation," in *Proceedings of the 43rd IEEE CDC, Paradise Island, Bahamas*, 2004.

[17] M. Breivik, "Nonlinear maneuvering control of underactuated ships," Master's thesis, Norwegian University of Science and Technology, 2003.

[18] K. D. Do and J. Pan, "Global tracking control of underactuated ships with off-diagonal terms," in *Proceedings of the 42nd IEEE CDC, Maui, Hawaii, USA*, 2003.

[19] A. Loría, "Cascaded nonlinear time-varying systems: Analysis and design," Lecture notes, Minicourse at IPM, Mexico, Tech. Rep., 2001.